A Related Works

Offline RL. Ensuring that the policy distribution remains close to the data distribution is crucial for offline RL, as distributional shift can lead to unreliable estimation (Levine et al., 2020). Offline RL algorithms typically fall into two categories to address this: those that enforce policy constraints on the learned policy (Wang et al., 2018; Fujimoto et al., 2019; Peng et al., 2019; Li et al., 2020; Fujimoto & Gu, 2021; Kostrikov et al., 2021; Chen et al., 2021; Emmons et al., 2021; Sun et al., 2024; Xu et al., 2023), and those that learn pessimistic value functions to penalize OOD actions (Kumar et al., 2020; Yu et al., 2020; An et al., 2021; Bai et al., 2022; Yang et al., 2022a; Ghasemipour et al., 2022; Sun et al., 2022a; Nikulin et al., 2023). Among these algorithms, ensemble-based approaches (An et al., 2021; Ghasemipour et al., 2022) demonstrate superior performance by estimating the lower-confidence bound (LCB) of Q values for OOD actions based on uncertainty estimation (Loquercio et al., 2020; Sun et al., 2022b). Additionally, imitation-based (Emmons et al., 2021) or weighted imitation-based algorithms (Wang et al., 2018; Nair et al., 2020; Kostrikov et al., 2021) generally enjoy better simplicity and stability compared to other pessimism-based approaches. Studies in offline goal-conditioned RL (Yang et al., 2023; 2022b) further demonstrate that weighted imitation learning offers improved generalization compared to pessimism-based offline RL methods. In addition to traditional offline RL methods, recent studies employ advanced techniques such as transformer (Chen et al., 2021; Chebotar et al., 2023; Yamagata et al., 2023) and diffusion models (Janner et al., 2022; Hansen-Estruch et al., 2023; Wang et al., 2022) for sequence modeling or function class enhancement, thereby increasing the potential of offline RL to tackle more challenging tasks.

Offline RL Theory. There is a large body of literature (Jin et al., 2021; Rashidinejad et al., 2021; Zanette et al., 2021; Xie et al., 2021a;b; Uehara & Sun, 2021; Shi et al., 2022; Zhong et al., 2022; Cui & Du, 2022; Xiong et al., 2022; Li et al., 2022; Cheng et al., 2022) dedicating to the development of pessimism-based algorithms for offline RL. These algorithms can provably efficiently find near-optimal policies with only the partial coverage condition. However, these works do not consider the corrupted data. Moreover, when the cumulative corruption level is sublinear, i.e., $\zeta = o(N)$, our algorithm can handle the corrupted data under similar partial coverage assumptions.

Robust RL. One type of robust RL is the distributionally robust RL, which aims to learn a policy that optimizes the worst-case performance across MDPs within an uncertainty set, typically framed as a Robust MDP problem (Nilim & Ghaoui, 2003; Iyengar, 2005; Ho et al., 2018; Moos et al., 2022). Hu et al. (2022) prove that distributionally robust RL can effectively reduce the sim-to-real gap. Besides, numerous studies in the online setting have explored robustness to perturbations on observations (Zhang et al., 2020; 2021), actions (Pinto et al., 2017; Tessler et al., 2019), rewards (Wang et al., 2020; Husain et al., 2021), and dynamics (Mankowitz et al., 2019). There is also a line of theory works (Lykouris et al., 2021; Wu et al., 2021; Wei et al., 2022; Ye et al., 2023a) studying online corruption-robust RL. In the offline setting, a number of works focus on testing-time robustness or distributional robustness in offline RL (Zhou et al., 2021; Shi & Chi, 2022; Hu et al., 2022; Yang et al., 2022a; Panaganti et al., 2022; Wen et al., 2023; Blanchet et al., 2023). Regarding the training-time robustness of offline RL, Li et al. (2023) investigated reward attacks in offline RL, revealing that certain dataset biases can implicitly enhance offline RL's resilience to reward corruption. Wu et al. (2022) propose a certification framework designed to ascertain the number of tolerable poisoning trajectories in relation to various certification criteria. From a theoretical perspective, Zhang et al. (2022) studied offline RL under contaminated data. One concurrent work (Ye et al., 2023b) leverages uncertainty weighting to tackle reward and dynamics corruption with theoretical guarantees. Different from prior work, we propose an algorithm that is both provable and practical under diverse data corruption on all elements.

Robust Imitation Learning. Robust imitation learning focuses on imitating the expert policy using corrupted demonstrations (Liu et al., 2022) or a mixture of expert and non-expert demonstrations (Wu et al., 2019; Tangkaratt et al., 2020b;a; Sasaki & Yamashina, 2020). These approaches primarily concentrate on noise or attacks on states and actions, without considering the future return. In contrast, robust offline RL faces the intricate challenges associated with corruption in rewards and dynamics.

Heavy-tailedness in RL. In the realm of RL, Zhuang & Sui (2021); Huang et al. (2023) delved into the issue of heavy-tailed rewards in tabular Markov Decision Processes (MDPs) and function approximation, respectively. There is also a line of works (Bubeck et al., 2013; Shao et al., 2018;

Xue et al., 2020; Zhong et al., 2021; Huang et al., 2022; Kang & Kim, 2023) studying the heavy-tailed bandit, which is a special case of MDPs. Besides, Garg et al. (2021) investigated the heavy-tailed gradients in the training of Proximal Policy Optimization. In contrast, our work addresses the heavy-tailed target distribution that emerges from data corruption.

Huber Loss in RL. The Huber loss, known for its robustness to outliers, has been widely employed in the Deep Q-Network (DQN) literature, (Dabney et al., 2018; Agarwal et al., 2020; Patterson et al., 2022). However, Ceron & Castro (2021) reevaluated the Huber loss and discovered that it fails to outperform the MSE loss on MinAtar environments. In our study, we leverage the Huber loss to address the heavy-tailedness in Q targets caused by data corruption, and we demonstrate its remarkable effectiveness.

B Algorithm Pseudocode

The pseudocode of RIQL and IQL can be found in Algorithm 1 and Algorithm 2, respectively:

Algorithm 1: Robust IQL algorithm

Initialize policy π_ϕ and value function V_ψ, $Q_{\theta_i}, i \in [1, K]$;
Normalize the observation according to Section 5.1 ;
for *training step*$= 1, 2, \ldots, T$ **do**
  Sample a mini-batch from the offline dataset: $\{(s, a, r, s')\} \sim D$;
  Update value function V_ψ to minimize

$$\mathcal{L}_V(\psi) = \mathbb{E}_{(s,a)\sim\mathcal{D}}\left[\mathcal{L}_2^\tau(Q_\alpha(s,a) - V_\psi(s))\right];$$

  Update $\{Q_{\theta_i}\}_{i=1}^K$ independently to minimize

$$\mathcal{L}_Q(\theta_i) = \mathbb{E}_{(s,a,r,s')\sim\mathcal{D}}[l_H^\delta(r + \gamma V_\psi(s') - Q_{\theta_i}(s,a))];$$

  Update policy π_ϕ to maximize

$$\mathcal{L}_\pi(\phi) = \mathbb{E}_{(s,a)\sim\mathcal{D}}\left[\exp(\beta A_\alpha(s,a))\log\pi_\phi(a|s)\right]$$

end for

Algorithm 2: IQL algorithm (Kostrikov et al., 2021) (for comparison)

Initialize policy π_ϕ and value function V_ψ, Q_θ ;
for *training step*$= 1, 2, \ldots, T$ **do**
  Sample a mini-batch from the offline dataset: $\{(s, a, r, s')\} \sim D$;
  Update value function V_ψ to minimize (2) ;
  Update Q_θ to minimize (1) ;
  Update policy π_ϕ to maximize (3)
end for

C Theoretical Analysis

C.1 Proof of Theorem 3

Before giving the proof of Theorem 3, we first state the performance difference lemma.

Lemma 6 (Performance Difference Lemma (Kakade & Langford, 2002))**.** *For any π and π', it holds that*

$$V^\pi - V^{\pi'} = \frac{1}{1-\gamma}\mathbb{E}_{s\sim d^\pi}\mathbb{E}_{a\sim\pi(\cdot|s)}[A^{\pi'}(s,a)].$$

Proof. See Kakade & Langford (2002) for a detailed proof. □

Proof of Theorem 3. First, we have

$$V^{\pi_{\mathrm{IQL}}} - V^{\tilde{\pi}_{\mathrm{IQL}}} = \underbrace{V^{\pi_{\mathrm{IQL}}} - V^{\pi_{\mathrm{E}}}}_{\text{imitation error 1}} + \underbrace{V^{\pi_{\mathrm{E}}} - V^{\tilde{\pi}_{\mathrm{E}}}}_{\text{corruption error}} + \underbrace{V^{\tilde{\pi}_{\mathrm{E}}} - V^{\tilde{\pi}_{\mathrm{IQL}}}}_{\text{imitation error 2}}.$$

We then analyze these three error terms respectively.

Corruption Error. By the performance difference lemma (Lemma 6), we have

$$\begin{aligned}
V^{\pi_{\mathrm{E}}} - V^{\tilde{\pi}_{\mathrm{E}}} &= -\frac{1}{1-\gamma}\mathbb{E}_{s\sim d^{\tilde{\pi}_{\mathrm{E}}}}\mathbb{E}_{a\sim\tilde{\pi}_{\mathrm{E}}(\cdot|s)}[A^{\pi_{\mathrm{E}}}(s,a)] \\
&= \frac{1}{1-\gamma}\mathbb{E}_{s\sim d^{\tilde{\pi}_{\mathrm{E}}}}\mathbb{E}_{a\sim\tilde{\pi}_{\mathrm{E}}(\cdot|s)}[V^{\pi_{\mathrm{E}}}(s) - Q^{\pi_{\mathrm{E}}}(s,a)] \\
&= \frac{1}{1-\gamma}\mathbb{E}_{s\sim d^{\tilde{\pi}_{\mathrm{E}}}}\left[\mathbb{E}_{a\sim\pi_{\mathrm{E}}(\cdot|s)}[Q^{\pi_{\mathrm{E}}}(s,a)] - \mathbb{E}_{a\sim\tilde{\pi}_{\mathrm{E}}(\cdot|s)}[Q^{\pi_{\mathrm{E}}}(s,a)]\right] \\
&\le \frac{R_{\max}}{(1-\gamma)^2}\mathbb{E}_{s\sim d^{\tilde{\pi}_{\mathrm{E}}}}[\|\tilde{\pi}_{\mathrm{E}}(\cdot\mid s) - \pi_{\mathrm{E}}(\cdot\mid s)\|_1],
\end{aligned} \tag{11}$$

where the second inequality uses the fact that $A^{\pi_{\mathrm{E}}}(s,a) = Q^{\pi_{\mathrm{E}}}(s,a) - V^{\pi_{\mathrm{E}}}(s)$, and the last inequality is obtained by Hölder's inequality and the fact that $\|Q^{\pi_{\mathrm{E}}}\|_\infty \le R_{\max}/(1-\gamma)$. By Pinsker's inequality, we further have

$$\begin{aligned}
\mathbb{E}_{s\sim d^{\tilde{\pi}_{\mathrm{E}}}}[\|\tilde{\pi}_{\mathrm{E}}(\cdot\mid s) - \pi_{\mathrm{E}}(\cdot\mid s)\|_1] &\le \mathbb{E}_{s\sim d^{\tilde{\pi}_{\mathrm{E}}}}\left[\sqrt{2\mathrm{KL}\big(\tilde{\pi}_{\mathrm{E}}(\cdot\mid s), \pi_{\mathrm{E}}(\cdot\mid s)\big)}\right] \\
&\le \sqrt{2\mathbb{E}_{(s,a)\sim d^{\tilde{\pi}_{\mathrm{E}}}}\log\frac{\tilde{\pi}_{\mathrm{E}}(a\mid s)}{\pi_{\mathrm{E}}(a\mid s)}} \\
&\le \sqrt{2M\mathbb{E}_{(s,a)\sim d_{\mathcal{D}}}\log\frac{\tilde{\pi}_{\mathrm{E}}(a\mid s)}{\pi_{\mathrm{E}}(a\mid s)}} \\
&= \sqrt{\frac{2M}{N}\sum_{i=1}^{N}\log\frac{\tilde{\pi}_{\mathrm{E}}(a_i\mid s_i)}{\pi_{\mathrm{E}}(a_i\mid s_i)}},
\end{aligned} \tag{12}$$

where the second inequality follows from Jensen's inequality and the definition of KL-divergence, the third inequality is obtained by the coverage assumption (Assumption 2) that $\sup_{s,a}[d^{\tilde{\pi}_{\mathrm{E}}}(s,a)/d_{\mathcal{D}}(s,a)] \le M$, and the last inequality uses the definition of $d_{\mathcal{D}}$. Recall that π_{E} and $\tilde{\pi}_{\mathrm{E}}$ take the following forms:

$$\begin{aligned}
\pi_{\mathrm{E}}(a\mid s) &\propto \pi_\mu(a\mid s)\cdot\exp(\beta\cdot[\mathcal{T}V^* - V^*](s,a)), \\
\tilde{\pi}_{\mathrm{E}}(a\mid s) &\propto \pi_{\mathcal{D}}(a\mid s)\cdot\exp(\beta\cdot[\tilde{\mathcal{T}}V^* - V^*](s,a)).
\end{aligned}$$

We have

$$\begin{aligned}
\frac{\tilde{\pi}_{\mathrm{E}}(a_i\mid s_i)}{\pi_{\mathrm{E}}(a_i\mid s_i)} = \frac{\pi_{\mathcal{D}}(a_i\mid s_i)\cdot\exp(\beta\cdot[\tilde{\mathcal{T}}V^* - V^*](s_i,a_i))}{\pi_\mu(a_i\mid s_i)\cdot\exp(\beta\cdot[\mathcal{T}V^* - V^*](s_i,a_i))} \\
\times\frac{\sum_{a\in A}\pi_\mu(a\mid s_i)\cdot\exp(\beta\cdot[\mathcal{T}V^* - V^*](s_i,a))}{\sum_{a\in A}\pi_{\mathcal{D}}(a\mid s_i)\cdot\exp(\beta\cdot[\tilde{\mathcal{T}}V^* - V^*](s_i,a))}.
\end{aligned} \tag{13}$$

By the definition of corruption levels in Assumption 1, we have

$$\zeta_i = \|[\mathcal{T}V](s_i,a) - [\tilde{\mathcal{T}}V](s_i,a)\|_\infty, \quad \max\left\{\frac{\pi_{\mathcal{D}}(a\mid s_i)}{\pi_\mu(a\mid s_i)}, \frac{\pi_\mu(a\mid s_i)}{\pi_{\mathcal{D}}(a\mid s_i)}\right\} \le \zeta_i', \quad \forall a\in A.$$

This implies that

$$\begin{aligned}
\frac{\pi_{\mathcal{D}}(a_i\mid s_i)\cdot\exp(\beta\cdot[\tilde{\mathcal{T}}V^* - V^*](s_i,a_i))}{\pi_\mu(a_i\mid s_i)\cdot\exp(\beta\cdot[\mathcal{T}V^* - V^*](s_i,a_i))} &\le \zeta_i'\cdot\exp(\beta\zeta_i) \\
\frac{\pi_\mu(a\mid s_i)\cdot\exp(\beta\cdot[\mathcal{T}V^* - V^*](s_i,a))}{\pi_{\mathcal{D}}(a\mid s_i)\cdot\exp(\beta\cdot[\tilde{\mathcal{T}}V^* - V^*](s_i,a))} &\le \zeta_i'\cdot\exp(\beta\zeta_i), \quad \forall a\in A.
\end{aligned} \tag{14}$$

Plugging (14) into (13), we have

$$\frac{\tilde{\pi}_{\mathrm{E}}(a_i \mid s_i)}{\pi_{\mathrm{E}}(a_i \mid s_i)} \leq \zeta_i' \cdot \exp(\beta\zeta_i) \cdot \frac{\zeta_i' \cdot \exp(\beta\zeta_i) \sum_{a\in A} \pi_{\mathcal{D}}(a \mid s_i) \cdot \exp(\beta \cdot [\tilde{\mathcal{T}}V^* - V^*](s_i, a))}{\sum_{a\in A} \pi_{\mathcal{D}}(a \mid s_i) \cdot \exp(\beta \cdot [\tilde{\mathcal{T}}V^* - V^*](s_i, a))}$$
$$= \zeta_i'^2 \cdot \exp(2\beta\zeta_i). \tag{15}$$

Combining (11), (12), and (15), we have

$$V^{\pi_{\mathrm{E}}} - V^{\tilde{\pi}_{\mathrm{E}}} \leq \frac{2R_{\max}}{(1-\gamma)^2}\sqrt{\frac{M}{N}\sum_{i=1}^{N}(\log\zeta_i' + 2\beta\zeta_i)} = \frac{2R_{\max}}{(1-\gamma)^2}\sqrt{\frac{M\zeta}{N}}, \tag{16}$$

where the last equality uses $\beta = 1$ and the definition of ζ in Assumption 1.

Imitation Error 1. Following the derivation of (11), we have

$$\begin{aligned} V^{\pi_{\mathrm{IQL}}} - V^{\pi_{\mathrm{E}}} &\leq \frac{R_{\max}}{(1-\gamma)^2}\mathbb{E}_{s\sim d^{\pi_{\mathrm{E}}}}[\|\pi_{\mathrm{E}}(\cdot \mid s) - \pi_{\mathrm{IQL}}(\cdot \mid s)\|_1] \\ &\leq \frac{\sqrt{2}R_{\max}}{(1-\gamma)^2}\mathbb{E}_{s\sim d^{\pi_{\mathrm{E}}}}[\sqrt{\mathrm{KL}(\pi_{\mathrm{E}}(\cdot \mid s), \pi_{\mathrm{IQL}}(\cdot \mid s))}] \\ &\leq \frac{\sqrt{2}R_{\max}}{(1-\gamma)^2}\sqrt{\mathbb{E}_{s\sim d^{\pi_{\mathrm{E}}}}[\mathrm{KL}(\pi_{\mathrm{E}}(\cdot \mid s), \pi_{\mathrm{IQL}}(\cdot \mid s))]} \\ &\leq \frac{\sqrt{2M}R_{\max}}{(1-\gamma)^2}\sqrt{\mathbb{E}_{s\sim\mu}[\mathrm{KL}(\pi_{\mathrm{E}}(\cdot \mid s), \pi_{\mathrm{IQL}}(\cdot \mid s))]} = \frac{\sqrt{2M}R_{\max}}{(1-\gamma)^2}\sqrt{\epsilon_1}, \end{aligned} \tag{17}$$

where the second inequality uses Pinsker's inequality, the third inequality is obtained by Jensen's inequality, the fourth inequality uses Assumption 2, and the final equality follows from the definition of ϵ_1.

Imitation Error 2. By the performance difference lemma (Lemma 6) and the same derivation of (11), we have

$$\begin{aligned} V^{\tilde{\pi}_{\mathrm{E}}} - V^{\tilde{\pi}_{\mathrm{IQL}}} &= \frac{R_{\max}}{1-\gamma}\mathbb{E}_{s\sim d^{\tilde{\pi}_{\mathrm{E}}}}\mathbb{E}_{a\sim\tilde{\pi}_{\mathrm{E}}(\cdot|s)}[A^{\tilde{\pi}_{\mathrm{IQL}}}(s,a)] \\ &\leq \frac{R_{\max}}{(1-\gamma)^2}\mathbb{E}_{s\sim d^{\tilde{\pi}_{\mathrm{E}}}}[\|\tilde{\pi}_{\mathrm{E}}(\cdot \mid s) - \tilde{\pi}_{\mathrm{IQL}}(\cdot \mid s)\|_1]. \end{aligned}$$

By the same derivation of (17), we have

$$V^{\tilde{\pi}_{\mathrm{E}}} - V^{\tilde{\pi}_{\mathrm{IQL}}} \leq \frac{\sqrt{2M}R_{\max}}{(1-\gamma)^2}\sqrt{\mathbb{E}_{s\sim\mathcal{D}}[\mathrm{KL}(\tilde{\pi}_{\mathrm{E}}(\cdot \mid s), \tilde{\pi}_{\mathrm{IQL}}(\cdot \mid s))]} \leq \frac{\sqrt{2M}R_{\max}}{(1-\gamma)^2}\sqrt{\epsilon_2}. \tag{18}$$

Putting Together. Combining (16), (17), and (18), we obtain that

$$V^{\pi_{\mathrm{IQL}}} - V^{\tilde{\pi}_{\mathrm{IQL}}} \leq \frac{\sqrt{2M}R_{\max}}{(1-\gamma)^2}[\sqrt{\epsilon_1} + \sqrt{\epsilon_2}] + \frac{2R_{\max}}{(1-\gamma)^2}\sqrt{\frac{M\zeta}{N}},$$

which concludes the proof of Theorem 3. □

Remark 7. *We would like to make a comparison with Zhang et al. (2022), a theory work about offline RL with corrupted data. They assume that ϵN data points are corrupted and propose a least-squares value iteration (LSVI) type algorithm that achieves an $\mathcal{O}(\sqrt{\epsilon})$ optimality gap by ignoring other parameters. When applying our results to their setting, we have $\zeta \leq \epsilon N$, which implies that our corruption error term $\mathcal{O}(\sqrt{\zeta/N}) \leq \mathcal{O}(\sqrt{\epsilon})$. This matches the result in Zhang et al. (2022), which combines LSVI with a robust regression oracle. However, their result may not readily apply to our scenario, given that we permit complete data corruption ($\epsilon = 1$). Furthermore, from the empirical side, IQL does not require any robust regression oracle and outperforms LSVI-type algorithms, such EDAC and MSG.*

C.2 Proof of Lemma 5

Proof of Lemma 5. We first state Theorem 1 of Sun et al. (2020) as follows.

Lemma 8 (Theorem 1 of Sun et al. (2020)). *Consider the following statistical model:*

$$y_i = \langle x_i, \beta^* \rangle + \varepsilon_i, \quad \textit{with } \mathbb{E}(\varepsilon_i \mid x_i) = 0, \mathbb{E}(|\varepsilon_i|^{1+\nu}) < \infty, \quad \forall 1 \le i \le N.$$

By solving the Huber regression problem with a proper parameter δ

$$\hat{\beta} = \arg\min_{\beta} \sum_{i=1}^{N} l_H^{\delta}(y_i - \langle x_i, \beta \rangle),$$

the obtained $\hat{\beta}$ satisfies

$$\|\hat{\beta} - \beta^*\|_2 \lesssim N^{-\min\{\nu/(1+\nu), 1/2\}}.$$

Back to our proof, for any $(s_i, a_i, s_i') \sim \mathcal{D}$, we take (i) $x_i = \mathbb{1}\{s_i, a_i\} \in \mathbb{R}^{|S \times A|}$ as the one-hot vector at (s_i, a_i) and (ii) $y_i = r_i + \gamma V_\psi(s_i')$. Moreover, we treat $\{r(s,a) + \gamma \mathbb{E}_{s' \sim P(\cdot|s,a)}[V_\psi(s')]\}_{(s,a) \in S \times A} \in \mathbb{R}^{|S \times A|}$ as β^*. Hence, by Lemma 8 and the fact that $\|\cdot\|_\infty \le \|\cdot\|_2$, we obtain

$$\|\hat{Q}(s,a) - r(s,a) - \gamma \mathbb{E}_{s' \sim P(\cdot|s,a)}[V_\psi(s')]\|_\infty \lesssim N^{-\min\{\nu/(1+\nu), 1/2\}},$$

where N is the size of dataset $\mathcal{D}$. This concludes the proof of Lemma 5. □

A Discussion about Recovering the Optimal Value Function We denote the optimal solutions to (2) and (7) by V_τ and Q_τ, respectively. When $N \to \infty$, we know

$$V_\tau(s) = \mathbb{E}^{\tau}_{a \sim \pi_{\mathcal{D}}(\cdot|s)}[Q_\tau(s,a)], \quad Q_\tau(s,a) = r(s,a) + \gamma \mathbb{E}_{s' \sim P(\cdot|s,a)}[V_\tau(s')],$$

where $\mathbb{E}^{\tau}_{x \sim X}[x]$ denotes the τ-th expectile of the random variable X. following the analysis of IQL (Kostrikov et al., 2021, Theorem 3), we can further show that $\lim_{\tau \to 1} V_\tau(s) = \max_{a \in \mathcal{A} \text{ s.t. } \pi_{\mathcal{D}}(a|s) > 0} Q^*(s,a)$. With the Huber loss, we can further recover the optimal value function even in the presence of a heavy-tailed target distribution.

D Implementation Details

D.1 Data Corruption Details

We apply both random and adversarial corruption to the four elements, namely states, actions, rewards, and dynamics (or "next-states"). In our experiments, we primarily utilize the "medium-replay-v2" and "medium-expert-v2" datasets from (Fu et al., 2020). These datasets are gathered either during the training of a SAC agent or by combining equal proportions of expert demonstrations and medium data, making them more representative of real-world scenarios. To control the cumulative corruption level, we introduce two parameters, c and ϵ. Here, c represents the corruption rate within the dataset of size N, while ϵ denotes the corruption scale for each dimension. We detail four types of random data corruption and a mixed corruption below:

- **Random observation attack**: We randomly sample $c \cdot N$ transitions (s, a, r, s'), and modify the state to $\hat{s} = s + \lambda \cdot \text{std}(s)$, $\lambda \sim \text{Uniform}[-\epsilon, \epsilon]^{d_s}$. Here, d_s represents the dimension of states and "std(s)" is the d_s-dimensional standard deviation of all states in the offline dataset. The noise is scaled according to the standard deviation of each dimension and is independently added to each respective dimension.
- **Random action attack**: We randomly select $c \cdot N$ transitions (s, a, r, s'), and modify the action to $\hat{a} = a + \lambda \cdot \text{std}(a)$, $\lambda \sim \text{Uniform}[-\epsilon, \epsilon]^{d_a}$, where d_a represents the dimension of actions and "std(a)" is the d_a-dimensional standard deviation of all actions in the offline dataset.

- **Random reward attack**: We randomly sample $c \cdot N$ transitions (s, a, r, s') from D, and modify the reward to $\hat{r} \sim \text{Uniform}[-30 \cdot \epsilon, 30 \cdot \epsilon]$. We multiply by 30 because we have noticed that offline RL algorithms tend to be resilient to small-scale random reward corruption (as observed in (Li et al., 2023)), but would fail when faced with large-scale random reward corruption.
- **Random dynamics attack**: We randomly sample $c \cdot N$ transitions (s, a, r, s'), and modify the next-step state $\hat{s}' = s' + \lambda \cdot \text{std}(s'), \lambda \sim \text{Uniform}[-\epsilon, \epsilon]^{d_s}$. Here, d_s indicates the dimension of states and "std(s')" is the d_s-dimensional standard deviation of all next-states in the offline dataset.
- **Random mixed attack**: We randomly select $c \cdot N$ of the transitions and execute the random observation attack. Subsequently, we again randomly sample $c \cdot N$ of the transitions and carry out the random action attack. The same process is repeated for both reward and dynamics attacks.

In addition, four types of adversarial data corruption are detailed as follows:

- **Adversarial observation attack**: We first pretrain an EDAC agent with a set of Q_p functions and a policy function π_p using clean dataset. Then, we randomly sample $c \cdot N$ transitions (s, a, r, s'), and modify the states to $\hat{s} = \min_{\hat{s} \in \mathbb{B}_d(s,\epsilon)} Q_p(\hat{s}, a)$. Here, $\mathbb{B}_d(s, \epsilon) = \{\hat{s} || \hat{s} - s| \leq \epsilon \cdot \text{std}(s)\}$ regularizes the maximum difference for each state dimension. The Q function in the objective is the average of the Q functions in EDAC. The optimization is implemented through Projected Gradient Descent similar to prior works (Madry et al., 2017; Zhang et al., 2020). Specifically, We first initialize a learnable vector $z \in [-\epsilon, \epsilon]^{d_s}$, and then conduct a 100-step gradient descent with a step size of 0.01 for $\hat{s} = s + z \cdot \text{std}(s)$, and clip each dimension of z within the range $[-\epsilon, \epsilon]$ after each update.
- **Adversarial action attack**: We use the pretrained EDAC agent with a group Q_p functions and a policy function π_p. Then, we randomly sample $c \cdot N$ transitions (s, a, r, s'), and modify the actions to $\hat{a} = \min_{\hat{a} \in \mathbb{B}_d(a,\epsilon)} Q_p(s, \hat{a})$. Here, $\mathbb{B}_d(a, \epsilon) = \{\hat{a} || \hat{a} - a| \leq \epsilon \cdot \text{std}(a)\}$ regularizes the maximum difference for each action dimension. The optimization is implemented through Projected Gradient Descent, as discussed above.
- **Adversarial reward attack**: We randomly sample $c \cdot N$ transitions (s, a, r, s'), and directly modify the rewards to: $\hat{r} = -\epsilon \times r$.
- **Adversarial dynamics attack**: We use the pretrained EDAC agent with a group of Q_p functions and a policy function π_p. Then, we randomly select $c \cdot N$ transitions (s, a, r, s'), and modify the next-step states to $\hat{s}' = \min_{\hat{s}' \in \mathbb{B}_d(s',\epsilon)} Q_p(\hat{s}', \pi_p(\hat{s}'))$. Here, $\mathbb{B}_d(s', \epsilon) = \{\hat{s}' || \hat{s}' - s'| \leq \epsilon \cdot \text{std}(s')\}$. The optimization is the same as discussed above.

Table 3: Hyperparameters used for RIQL under the random corruption benchmark.

Environments	Attack Element	N	α	δ
Halfcheetah	observation	5	0.1	0.1
	action	3	0.25	0.5
	reward	5	0.25	3.0
	dynamics	5	0.25	3.0
Walker2d	observation	5	0.25	0.1
	action	5	0.1	0.5
	reward	5	0.1	3.0
	dynamics	3	0.25	1.0
Hopper	observation	3	0.25	0.1
	action	5	0.25	0.1
	reward	3	0.25	1.0
	dynamics	5	0.5	1.0

D.2 Implementation Details of IQL and RIQL

For the policy and value networks of IQL and RIQL, we utilize an MLP with 2 hidden layers, each consisting of 256 units, and ReLU activations. These neural networks are updated using the Adam

Table 4: Hyperparameters used for RIQL under the adversarial corruption benchmark.

Environments	Attack Element	N	α	δ
Halfcheetah	observation	5	0.1	0.1
	action	5	0.1	1.0
	reward	5	0.1	1.0
	dynamics	5	0.1	1.0
Walker2d	observation	5	0.25	1.0
	action	5	0.1	1.0
	reward	5	0.1	3.0
	dynamics	5	0.25	1.0
Hopper	observation	5	0.25	1.0
	action	5	0.25	1.0
	reward	5	0.25	0.1
	dynamics	5	0.5	1.0

optimizer with a learning rate of 3×10^{-4}. We set the discount factor as $\gamma = 0.99$, the target networks are updated with a smoothing factor of 0.005 for soft updates. The hyperparameter β and τ for IQL and RIQL are set to 3.0 and 0.7 across all experiments. In terms of policy parameterization, we argue that RIQL is robust to different policy parameterizations, such as deterministic policy and diagonal Gaussian policy. For the main results, IQL and RIQL employ a deterministic policy, which means that maximizing the weighted log-likelihood is equivalent to minimizing a weighted l_2 loss on the policy output: $\mathcal{L}_\pi(\phi) = \mathbb{E}_{(s,a)\sim\mathcal{D}}[\exp(\beta A(s,a))\|a - \pi_\phi(s)\|_2^2]$. We also include a discussion about the diagonal Gaussian parameterization in Appendix E.4. In the training phase, we train IQL, RIQL, and other baselines for 3×10^6 steps following (An et al., 2021), which corresponds to 3000 epochs with 1000 steps per epoch. The training is performed using a batch size of 256. For evaluation, we rollout each agent in the clean environment for 10 trajectories (maximum length equals 1000) and average the returns. All reported results are averaged over four random seeds. As for the specific hyperparameters of RIQL, we search $K \in \{3, \mathbf{5}\}$ and quantile $\alpha \in \{\mathbf{0.1}, \mathbf{0.25}, 0.5\}$ for the quantile Q estimator, and $\delta \in \{\mathbf{0.1}, 0.5, \mathbf{1.0}, 3.0\}$ for the Huber loss. In most settings, we find that the highlighted hyperparameters often yield the best results. The specific hyperparameters used for the random and adversarial corruption experiment in Section 6.1 are listed in Table 3 and Table 4, respectively. Our code is available at https://github.com/YangRui2015/RIQL, which is based on the open-source library of CORL (Tarasov et al., 2022).

D.3 Quantile Calculation

To calculate the α-quantile for a group of Q function $\{Q_{\theta_i}\}_{i=1}^K$, we can map $\alpha \in [0, 1]$ to the range of indices $[1, K]$ in order to determine the location of the quantile in the sorted input. If the quantile lies between two data points $Q_{\theta_i} < Q_{\theta_j}$ with indices i, j in the sorted order, the result is computed according to the linear interpolation: $Q_\alpha = Q_{\theta_i} + (Q_{\theta_j} - Q_{\theta_i}) * \text{fraction}(\alpha \times (K-1)+1)$, where the "fraction" represents the fractional part of the computed index. As a special case, when $K = 2$, $Q_\alpha = (1-\alpha)\min(Q_{\theta_0}, Q_{\theta_1}) + \alpha\max(Q_{\theta_0}, Q_{\theta_1})$, and Q_α recovers the Clipped Double Q-learning trick when $\alpha = 0$.

E Additional Experiments

E.1 Ablation of IQL

As observed in Figure 1, IQL demonstrates notable robustness against some types of data corruption. However, it raises the question: **which component of IQL contributes most to its robustness?** IQL can be interpreted as a combination of expectile regression and weighted imitation learning. To understand the contribution of each component, we perform an ablation study on IQL under mixed corruption in the Hopper and Walker tasks, setting the corruption rate to 0.1 and the corruption scale to 1.0. Specifically, we consider the following variants:

IQL τ = 0.7: This is the standard IQL baseline.

IQL τ = 0.5: This variant sets $\tau = 0.5$ for IQL.

IQL w/o Expectile: This variant removes the expectile regression that learns the value function and instead directly learns the Q function to minimize $\mathbb{E}_{(s,a,r,s')\sim\mathcal{D}}[(r+\gamma Q(s',\pi(s'))-Q(s,a))^2]$, and updating the policy to maximize $\mathbb{E}_{(s,a)\sim\mathcal{D}}[\exp(Q(s,a)-Q(s,\pi(s)))\log\pi(a|s)]$.

ER w. Q gradient: This variant retains the expectile regression to learn the Q function and V function, then uses only the learned Q function to perform a deterministic policy gradient: $\max_\pi[Q(s,\pi(s))]$.

The results are presented in Figure 8. From these, we can conclude that while expectile regression enhances performance, it is not the key factor for robustness. On the one hand, **IQL τ = 0.7** outperforms **IQL τ = 0.5** and **IQL w/o Expectile**, confirming that expectile regression is indeed an enhancement factor. On the other hand, the performance of **ER w. Q gradient** drops to nearly zero, significantly lower than BC, indicating that expectile regression is not the crucial component for robustness. Instead, the supervised policy learning scheme is proved to be the key to achieving better robustness.

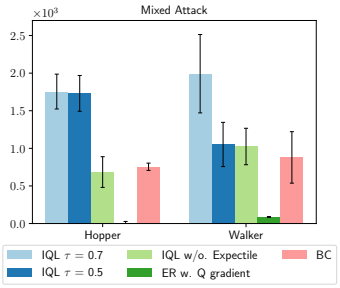

Figure 8: Ablation results of IQL under mixed attack.

E.2 Ablation of Observation Normalization

Figure 9 illustrates the comparison between IQL and "IQL (norm)" on the medium-replay and medium-expert datasets under various data corruption scenarios. In most settings, IQL with normalization surpasses the performance of the standard IQL. This finding contrasts with the general offline Reinforcement Learning (RL) setting, where normalization does not significantly enhance performance, as noted by (Fujimoto & Gu, 2021). These results further justify our decision to incorporate observation normalization into RIQL.

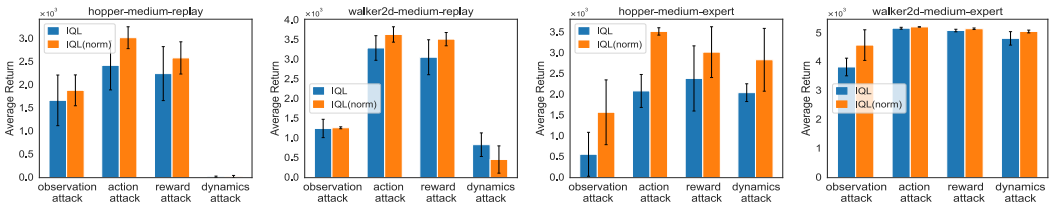

(a) (b) (c) (d)

Figure 9: Comparison of IQL w/ and w/o observation normalization.

E.3 Evaluation under the Mixed Corruption

We conducted experiments under mixed corruption settings, where corruption independently occurred on four elements: state, actions, rewards, and next-states (or dynamics). The results for corruption rates of 0.1/0.2 and corruption scales of 1.0/2.0 on the "medium-replay" datasets are presented in Figure 10 and Figure 11. From the figures, it is evident that **RIQL consistently outperforms other baselines by a significant margin in the mixed attack settings with varying corruption rates and scales**. Among the baselines, EDAC and MSG continue to struggle in this corruption setting. Besides, CQL also serves as a reasonable baseline, nearly matching the performance of IQL in such mixed corruption settings. Additionally, SQL also works reasonably under a small corruption rate of 0.1 but fails under a corruption rate of 0.2.

E.4 Evaluation of Different Policy Parameterization

In the official implementation of IQL (Kostrikov et al., 2021), the policy is parameterized as a diagonal Gaussian distribution with a state-independent standard deviation. However, in the data corruption setting, our findings indicate that this version of IQL generally underperforms IQL with a deterministic policy. This observation is supported by Figure 12, where we compare the performance under the mixed attack with a corruption rate of 0.1. Consequently, we use the deterministic

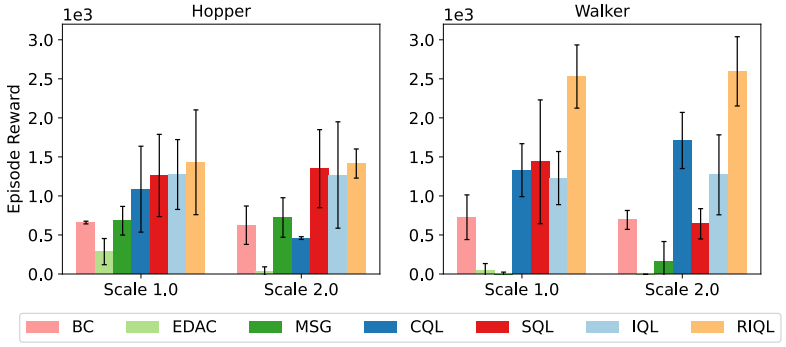

Figure 10: Results under random mixed attack with a corruption rate of 0.1.

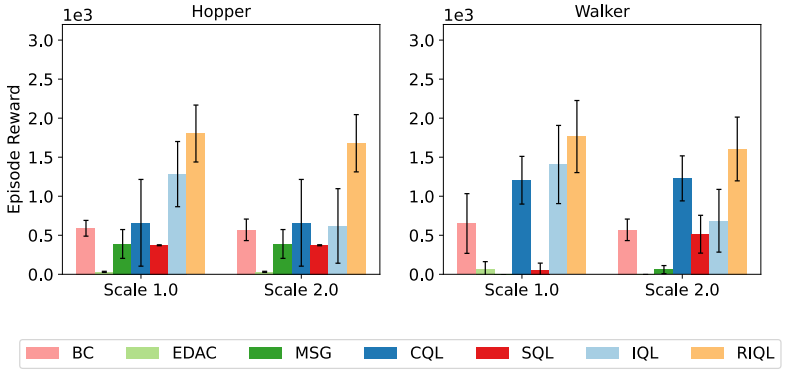

Figure 11: Results under random mixed attack with a corruption rate of 0.2.

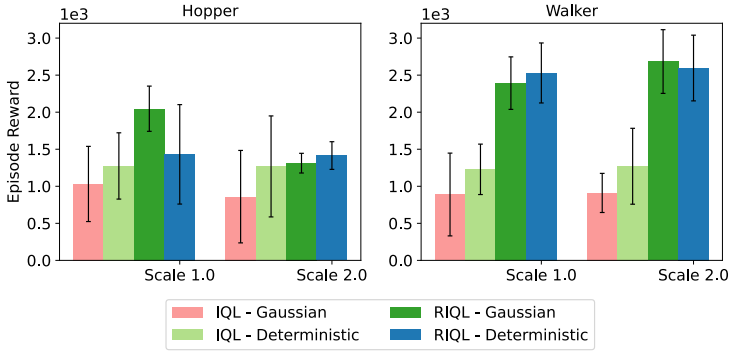

Figure 12: Comparison of different policy parameterizations under random mixed attack with a corruption rate of 0.1.

policy for both IQL and RIQL by default. Intriguingly, **RIQL demonstrates greater robustness to the policy parameterization**. In Figure 12, "RIQL - Gaussian" can even surpass "RIQL - Deterministic" and exhibits lower performance variance. We also note the consistent improvement of RIQL over IQL under different policy parameterizations, which serves as an additional advantage of RIQL. Based on our extensive experiments, we have noticed that "RIQL - Gaussian" offers greater stability and necessitates less hyperparameter tuning than "RIQL - Deterministic". Conversely, "RIQL - Deterministic" requires more careful hyperparameter tuning but can yield better results on average in scenarios with higher corruption rates.

Table 5: Average normalized performance under random data corruption (scale 1.0) using **"medium-expert" datasets**. Results are averaged over 4 random seeds.

Environment	Attack Element	BC	EDAC	MSG	CQL	SQL	IQL	RIQL (ours)
Halfcheetah	observation	51.6±2.9	-4.0±3.2	-4.9±4.5	3.4±1.6	30.5±5.1	71.0±3.4	**79.7±7.2**
	action	61.2±5.6	45.4±3.2	32.8±4.1	67.5±9.7	89.8±0.4	88.6±1.2	**92.9±0.6**
	reward	59.9±3.3	51.8±6.6	28.7±6.0	87.3±5.1	92.9±0.7	**93.4±1.2**	93.2±0.5
	dynamics	59.9±3.3	25.4±11.3	2.5±2.4	54.0±1.9	78.3±3.2	80.4±2.0	**92.2±0.9**
Walker2d	observation	**106.2±1.7**	-0.4±0.0	-0.3±0.1	15.0±2.6	17.5±4.3	71.1±23.5	101.3±11.8
	action	89.5±17.3	48.4±20.5	3.8±1.7	109.2±0.3	109.7±0.7	112.7±0.5	**113.5±0.5**
	reward	97.9±15.4	35.0±29.8	-0.4±0.3	104.2±5.4	110.1±0.4	110.7±1.3	**112.7±0.6**
	dynamics	97.9±15.4	0.2±0.5	3.6±6.7	82.0±11.9	93.5±3.7	100.3±7.5	**112.8±0.2**
Hopper	observation	52.7±1.6	0.8±0.0	0.9±0.1	46.2±12.9	1.3±0.1	23.2±33.6	**76.2±24.2**
	action	50.4±1.5	23.5±6.0	18.8±10.6	83.5±13.5	59.1±32.0	77.8±16.4	**92.6±38.9**
	reward	52.4±1.5	0.7±0.0	3.9±5.4	90.8±3.6	85.4±16.3	78.6±31.0	**91.4±25.9**
	dynamics	52.4±1.5	5.6±6.5	2.1±2.4	26.7±7.5	75.8±9.3	69.7±25.3	**84.6±15.4**
Average score ↑		69.3	19.4	7.6	64.2	70.3	81.5	**95.3**

E.5 Evaluation on the Medium-expert Datasets

In addition to the "medium-replay" dataset, which closely resembles real-world environments, we also present results using the "medium-expert" dataset under random corruption in Table 5. The "medium-expert" dataset is a mixture of 50% expert and 50% medium demonstrations. As a result of the inclusion of expert demonstrations, the overall performance of each algorithm is much better compared to the results obtained from the "medium-replay" datasets. Similar to the main results, EDAC and MSG exhibit very low average scores across various data corruption scenarios. Additionally, CQL and SQL only manage to match the performance of BC. IQL, on the other hand, outperforms BC by 17.6%, confirming its effectiveness. Most notably, **RIQL achieves the highest score in 10 out of 12 settings and improves by** 16.9% **over IQL**. These results align with our findings in the main paper, further demonstrating the superior effectiveness of RIQL across different types of datasets.

Table 6: Average normalized performance under **random corruption of scale 2.0** using the "medium-replay" datasets. Results are averaged over 4 random seeds.

Environment	Attack Element	BC	EDAC	MSG	CQL	SQL	IQL	RIQL (ours)
Walker2d	observation	16.1±5.5	-0.4±0.0	-0.4±0.1	12.5±21.4	0.7±1.2	27.4±5.7	**50.3±11.5**
	action	13.3±2.5	77.5±3.4	16.3±3.7	15.4±9.1	79.0±5.2	69.9±2.8	**82.9±3.8**
	reward	16.0±7.4	1.2±1.6	9.3±5.9	48.4±4.6	0.2±0.9	56.0±7.4	**81.5±4.6**
	dynamics	16.0±7.4	-0.1±0.0	4.2±3.8	0.1±0.4	18.5±3.6	12.0±5.6	**77.8±6.3**
Hopper	observation	17.6±1.2	2.7±0.8	7.1±5.8	29.2±1.9	13.7±3.1	**69.7±7.0**	55.8±17.4
	action	16.0±3.1	31.9±3.2	35.9±8.3	19.2±0.5	38.8±1.7	75.1±18.2	**92.7±11.0**
	reward	19.5±3.4	6.4±5.0	42.1±14.2	51.7±14.8	41.5±4.2	62.1±8.3	**85.0±17.3**
	dynamics	19.5±3.4	0.8±0.0	3.7±3.2	0.8±0.1	14.4±2.7	0.9±0.3	**45.8±9.3**
Average score ↑		16.8	15.0	14.8	22.2	25.9	46.6	**71.6**

Table 7: Average normalized performance under **adversarial corruption of scale 2.0** using the "medium-replay" datasets. Results are averaged over 4 random seeds.

Environment	Attack Element	BC	EDAC	MSG	CQL	SQL	IQL	RIQL (ours)
Walker2d	observation	13.0±1.5	3.9±6.7	3.5±3.9	63.3±5.1	2.7±3.0	47.0±8.3	**71.5±6.4**
	action	0.3±0.5	**9.2±2.4**	4.8±0.4	1.7±3.5	5.6±1.4	3.0±0.9	7.9±0.5
	reward	16.0±7.4	-0.1±0.0	9.1±3.8	28.4±19.2	-0.3±0.0	22.9±12.5	**81.1±2.4**
	dynamics	16.0±7.4	2.2±1.8	1.9±0.2	4.2±2.2	3.4±1.9	1.7±1.0	**66.0±7.7**
Hopper	observation	17.0±5.4	23.9±10.6	19.9±6.6	52.6±8.8	14.0±1.2	44.3±2.9	**57.0±7.6**
	action	9.9±4.6	23.3±4.7	22.8±1.7	14.7±0.9	19.3±3.1	21.8±4.9	**23.8±4.0**
	reward	19.5±3.4	1.2±0.5	22.9±1.1	22.9±1.1	0.6±0.0	24.7±1.6	**35.5±6.7**
	dynamics	19.5±3.4	0.6±0.0	0.6±0.0	0.6±0.0	24.3±3.2	0.7±0.0	**29.9±1.5**
Average score ↑		13.9	8.0	10.7	23.6	8.7	20.8	**46.6**

E.6 Evaluation under Large-scale Corruption

In our main results, we focused on random and adversarial corruption with a scale of 1.0. In this subsection, we present an empirical evaluation under a corruption scale of 2.0 using the "medium-replay" datasets. The results for random and adversarial corruptions are presented in Table 6 and Table 7, respectively.

In both tables, **RIQL achieves the highest performance in 7 out of 8 settings, surpassing IQL by** 53.5% **and** 124.0%, respectively. Most algorithms experience a significant decrease in performance under adversarial corruption at the same scale, with the exception of CQL. However, it is still not comparable to our algorithm, RIQL. These results highlight the superiority of RIQL in handling large-scale random and adversarial corruptions.

E.7 Training Time

We report the average epoch time on the Hopper task as a measure of computational cost in Table 8. From the table, it is evident that BC requires the least training time, as it has the simplest algorithm design. IQL requires more than twice the amount of time compared to BC, as it incorporates expectile regression and weighted imitation learning. Additionally, RIQL requires a comparable computational cost to IQL, introducing the Huber loss and quantile Q estimators. On the other hand, EDAC, MSG, and CQL require significantly longer training time. This is primarily due to their reliance on a larger number of Q ensembles and additional computationally intensive processes, such as the approximate logsumexp via sampling in CQL. Notably, DT necessitates the longest epoch time, due to its extensive transformer-based architecture. The results indicate that RIQL achieves significant gains in robustness without imposing heavy computational costs.

Table 8: Average Epoch Time.

Algorithm	BC	DT	EDAC	MSG	CQL	IQL	RIQL
Time (s)	3.8±0.1	28.9±0.2	14.1±0.3	12.0±0.8	22.8±0.7	8.7±0.3	9.2±0.4

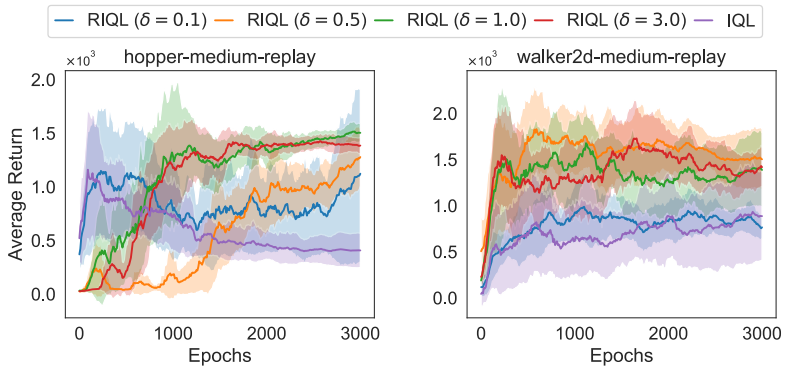

Figure 13: Hyperparameter study for δ in the Huber loss under the mixed attack.

E.8 Hyperparameter Study

In this subsection, we investigate the impact of key hyperparameters in RIQL, namely δ in the Huber loss, and α, K in the quantile Q estimators. We conduct our experiments using the mixed attack, where corruption is independently applied to each element (states, actions, rewards, and next-states) with a corruption rate of 0.2 and a corruption scale of 1.0. The dataset used for this evaluation is the "medium-replay" dataset of the Hopper and Walker environments.

Hyperparameter δ In this evaluation, we set $\alpha = 0.1$ and $K = 5$ for RIQL. The value of δ directly affects the position of the boundary between the l_1 loss and the l_2 loss. As δ approaches

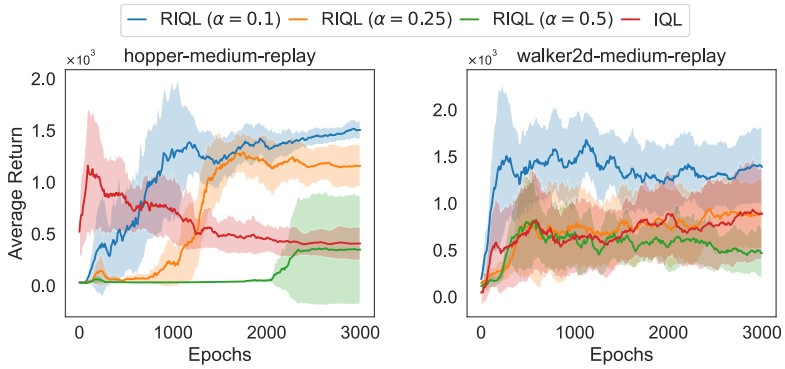

Figure 14: Hyperparameter study for α in the quantile estimators under the mixed attack.

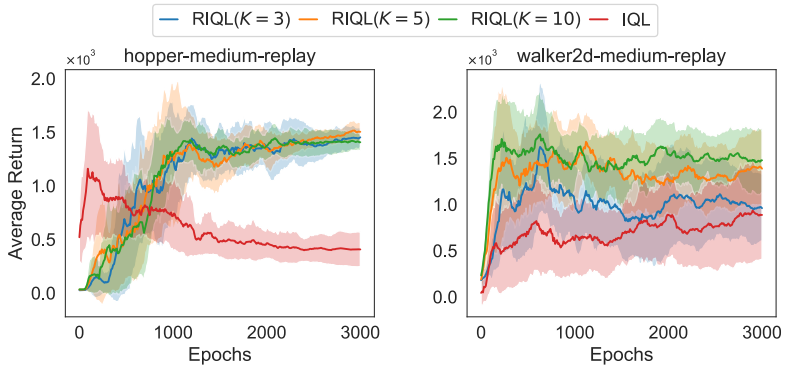

Figure 15: Hyperparameter study for K in the quantile estimators under the mixed attack.

0, the boundary moves far from the origin of coordinates, making the loss function similar to the squared loss and resulting in performance closer to IQL. This can be observed in Figure 13, where $\delta = 0.1$ is the closest to IQL. As δ increases, the Huber loss becomes more similar to the l_1 loss and exhibits greater robustness to heavy-tail distributions. However, excessively large values of δ can decrease performance, as the l_1 loss can also impact the convergence. This is evident in the results, where $\delta = 3.0$ slightly decreases performance. Generally, $\delta = 1.0$ achieves the best or nearly the best performance in the mixed corruption setting. However, it is important to note that the optimal value of δ also depends on the corruption type when only one type of corruption (e.g., state, action, reward, and next-state) takes place. For instance, we find that $\delta = 0.1$ generally yields the best results for state and action corruption, while $\delta = 1$ is generally optimal for the dynamics corruption.

Hyperparameter α In this evaluation, we set $\delta = 1.0$ and $K = 5$ for RIQL. The value of α determines the quantile used for estimating Q values and advantage values. A small α results in a higher penalty for the corrupted data, generally leading to better performance. This is evident in Figure 14, where $\alpha = 0.1$ achieves the best performance in the mixed corruption setting. However, as mentioned in Section 5.3, when only dynamics corruption is present, it is advisable to use a slightly larger α, such as 0.25, to prevent the excessive pessimism in the face of dynamics corruption.

Hyperparameter K In this evaluation, we set $\alpha = 0.1$ and $\delta = 1.0$ for RIQL. Hyperparameter K is used to adjust the quantile Q estimator for in-dataset penalty. From Figure 15, we can observe that the impact of K is more pronounced in the walker2d task compared to the hopper task, whereas the above hyperparameter α has a greater influence on the hopper task. For the walker2d task, a larger value of K leads to better performance. Overall, $K = 5$ achieves the best or nearly the best performance in both settings. Therefore, we set $K = 5$ by default, considering both computational cost and performance.

Table 9: Comparison with **additional baselines under random data corruption**. Average normalized scores are reported and the highest score is highlighted.

Environment	Attack Element	DT	MSG	UWMSG	RIQL (ours)
Halfcheetah	observation	**33.7±1.9**	-0.2±2.2	2.1±0.4	27.3±2.4
	action	36.3±1.5	52.0±0.9	**53.8±0.6**	42.9±0.6
	reward	39.2±1.0	17.5±16.4	39.9±1.8	**43.6±0.6**
	dynamics	33.7±1.9	1.7±0.4	3.6±2.0	**43.1±0.2**
Walker2d	observation	**54.5±5.0**	-0.4±0.1	1.5±2.0	28.4±7.7
	action	10.3±3.1	25.3±10.6	61.2±9.9	**84.6±3.3**
	reward	65.5±4.9	18.4±9.5	65.9±13.9	**83.2±2.6**
	dynamics	54.5±5.0	7.4±3.7	6.5±2.8	**78.2±1.8**
Hopper	observation	**65.2±12.1**	6.9±5.0	11.3±4.0	62.4±1.8
	action	15.5±0.7	37.6±6.5	82.0±17.6	**90.6±5.6**
	reward	78.0±5.3	24.9±4.3	61.0±19.5	**84.8±13.1**
	dynamics	**65.2±12.1**	12.4±4.9	18.7±4.6	51.5±8.1
Average score ↑		46.0	17.0	34.0	**60.0**

E.9 Additional Baselines

In addition to the baselines compared in the main paper, we compare RIQL to a sequence-modeling baseline, Decision Transformer (DT) (Chen et al., 2021), and a recently proposed robust offline RL algorithm for data corruption, UWMSG (Ye et al., 2023b). The results are presented in Table 9 and Table 10. Overall, RIQL demonstrates robust performance compared to the two additional baselines.

In comparison to BC, DT demonstrates a notable improvement, highlighting the effectiveness of sequence modeling. Furthermore, as DT employs a distinct sequence modeling approach from TD-based methods, it does not store data in independent transitions $\{s_i, a_i, r_i, s'_i\}_{i=1}^N$. Instead, it utilizes a trajectory sequence $\{s_t^i, a_t^i, r_t^i\}_{t=1}^T$ for i-th trajectory. Consequently, the observation corruption and dynamics corruption are identical for DT. Analyzing Table 9 and Table 10, we can observe that DT holds an advantage under observation corruption due to its ability to condition on historical information rather than relying solely on a single state. Despite leveraging trajectory history information and requiring 3.1 times the epoch time compared to RIQL, DT still falls significantly behind RIQL in performance under both random and adversarial data corruption. Exploring the incorporation of trajectory history, similar to DT, into RIQL could be a promising avenue for future research.

With regard to UWMSG, we observe its improvement over MSG, confirming its effectiveness with uncertainty weighting. However, it is still more vulnerable to data corruption compared to RIQL. We speculate that the explicit uncertainty estimation used in UWMSG is still unstable.

Table 10: Comparison with **additional baselines under adversarial data corruption**. Average normalized scores are reported and the highest score is highlighted.

Environment	Attack Element	DT	MSG	UWMSG	RIQL (ours)
Halfcheetah	observation	35.5±4.3	1.1±0.2	1.3±0.8	**35.7±4.2**
	action	16.6±1.2	37.3±0.7	**39.4±3.1**	31.7±1.7
	reward	37.0±2.6	**47.7±0.4**	43.8±0.8	44.1±0.8
	dynamics	35.5±4.3	-1.5±0.0	10.9±1.8	**35.8±2.1**
Walker2d	observation	57.4±3.2	2.9±2.7	9.9±1.5	**70.0±5.3**
	action	9.5±1.6	5.4±0.9	7.4±2.4	**66.1±4.6**
	reward	64.9±5.4	9.6±4.9	52.9±12.1	**85.0±1.5**
	dynamics	57.4±3.2	0.1±0.2	2.1±0.2	**60.6±21.8**
Hopper	observation	**57.7±15.1**	16.0±2.8	13.6±0.7	50.8±7.6
	action	14.0±1.1	23.0±2.1	34.0±4.4	**63.6±7.3**
	reward	**68.6±10.5**	22.6±2.8	23.6±2.1	65.8±9.8
	dynamics	57.7±15.1	0.6±0.0	0.8±0.0	**65.7±21.1**
Average score ↑		42.7	13.7	20.0	**56.2**

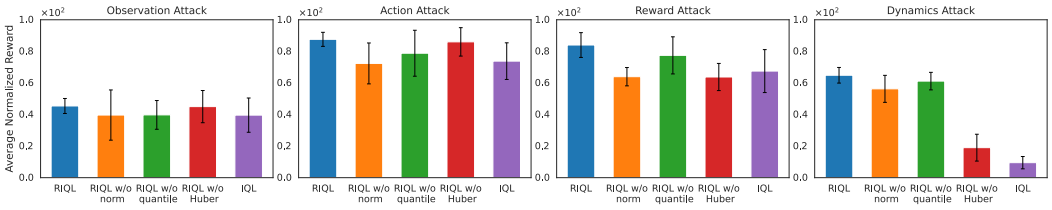

Figure 16: Ablations of RIQL under four types of data corruption.

E.10 Additional Ablation Study

In this subsection, we analyze the contributions of RILQ's components in the presence of observation, action, reward, and dynamics corruption. Figure 16 illustrates the average normalized performance of Walker and Hopper tasks on the medium-replay datasets. We consider three variants of RIQL: RIQL without observation normalization (**RIQL w/o norm**), RIQL without the quantile Q estimator (**RIQL w/o quantile**), and RIQL without the Huber loss (**RIQL w/o Huber**). In **RIQL w/o quantile**, the Clipped Double Q trick used in IQL, is employed to replace the quantile Q estimator in RIQL. Based on the figure, we draw the following conclusions for each component: (1) normalization is beneficial for all four types of corruption, (2) quantile Q estimator is more effective for observation and action corruption but less so for reward and dynamics corruption, (3) conversely, the Huber loss is more useful for reward and dynamics corruption but less effective for observation and action corruption. Overall, all three components contribute to the performance of RIQL.

F Evaluation on AntMaze Tasks

In this section, we present the evaluation of RIQL and baselines on a more challenging benchmark, AntMaze, which introduces additional difficulties due to its sparse-reward setting. Specifically, we assess four "medium" and "large" level tasks. Similar to the MuJoCo tasks, we consider random data corruption, but with a corruption rate of 0.2 for all AntMaze tasks. We observe that algorithms in AntMaze tasks are more sensitive to data noise, particularly when it comes to observation and dynamics corruption. Therefore, we use smaller corruption scales for observation (0.3), action (1.0), reward (30.0), and dynamics (0.3). The hyperparameters used for RIQL are list in Talbe 12.

As shown in Table 11, methods such as BC, DT, EDAC, and CQL struggle to learn meaningful policies in the presence of data corruption. In contrast, IQL exhibits relatively higher robustness, particularly under action corruption. RIQL demonstrates a significant improvement of 77.8% over IQL, successfully learning reasonable policies even in the presence of all types of corruption. These results further strengthen the findings in our paper and highlight the importance of RIQL.

Table 11: Average normalized performance under random data corruption on AntMaze tasks.

Environment	Attack Element	BC	DT	EDAC	CQL	IQL	RIQL (ours)
antmaze-medium-play-v2	observation	0.0±0.0	0.0±0.0	0.0±0.0	0.8±1.4	7.4±5.0	**18.0 ± 4.7**
	action	0.0±0.0	0.0±0.0	0.0±0.0	0.8±1.4	63.5 ± 5.4	**64.6 ± 5.2**
	reward	0.0±0.0	0.0±0.0	0.0±0.0	0.0±0.0	12.4 ± 8.1	**61.0 ± 5.8**
	dynamics	0.0±0.0	0.0±0.0	0.0±0.0	37.5±28.6	32.7 ± 8.4	**63.2 ± 5.4**
antmaze-medium-diverse-v2	observation	0.0±0.0	0.0±0.0	0.0±0.0	0.0±0.0	11.9 ± 6.9	**12.5 ± 7.9**
	action	0.0±0.0	0.0±0.0	0.0±0.0	15.0±22.3	**65.6 ± 4.6**	62.3 ± 5.5
	reward	0.0±0.0	0.0±0.0	0.0±0.0	0.0±0.0	8.3 ± 4.5	**22.9 ± 17.9**
	dynamics	0.0±0.0	0.0±0.0	0.0±0.0	20.8±14.2	35.5 ± 8.5	**41.8 ± 7.2**
antmaze-large-play-v2	observation	0.0±0.0	0.0±0.0	0.0±0.0	0.0±0.0	0.0±0.0	**27.3 ± 5.1**
	action	0.0±0.0	0.0±0.0	0.0±0.0	0.0±0.0	33.1 ± 6.2	**33.2 ± 6.3**
	reward	0.0±0.0	0.0±0.0	0.0±0.0	0.0±0.0	0.6 ± 0.9	**27.7 ± 8.0**
	dynamics	0.0±0.0	0.0±0.0	0.0±0.0	4.2±5.5	1.6 ± 1.5	**25.0 ± 6.4**
antmaze-large-diverse-v2	observation	0.0±0.0	0.0±0.0	0.0±0.0	0.0±0.0	0.0±0.0	**24.9±10.7**
	action	0.0±0.0	0.0±0.0	0.0±0.0	0.0±0.0	**33.7 ± 5.9**	30.9 ± 9.4
	reward	0.0±0.0	0.0±0.0	0.0±0.0	0.0±0.0	1.1 ± 1.1	**20.2 ± 17.0**
	dynamics	0.0±0.0	0.0±0.0	0.0±0.0	4.2±7.2	2.5 ± 2.9	**16.5±5.7**
Average score ↑		0.0	0.0	0.0	5.2	19.4	**34.5**

Table 12: Hyperparameters used for RIQL under the random corruption on the AntMaze Tasks.

Environments	Attack Element	N	α	δ
antmaze-medium-play-v2	observation	5	0.25	0.5
	action	3	0.5	0.1
	reward	3	0.5	0.5
	dynamics	3	0.5	0.5
antmaze-medium-diverse-v2	observation	3	0.25	0.1
	action	3	0.5	0.1
	reward	3	0.25	0.1
	dynamics	3	0.5	0.1
antmaze-large-play-v2	observation	3	0.25	0.5
	action	3	0.25	0.1
	reward	3	0.5	0.5
	dynamics	3	0.5	1.0
antmaze-large-diverse-v2	observation	3	0.25	0.5
	action	5	0.25	0.05
	reward	3	0.25	0.5
	dynamics	3	0.5	0.5

F.1 Learning Curves of the Benchmark Experiments

In Figure 17 and Figure 18, we present the learning curves of RIQL and other baselines on the "medium-replay" datasets, showcasing their performance against random and adversarial corruption, respectively. The corruption rate is set to 0.3 and the corruption scale is set to 1.0. These results correspond to Section 6.1 in the main paper. From these figures, it is evident that RIQL not only attains top-level performance but also exhibits remarkable learning stability compared to other baselines that can experience significant performance degradation during training. We postulate that this is attributed to the inherent characteristics of the Bellman backup, which can accumulate errors along the trajectory throughout the training process, particularly under the data corruption setting. On the contrary, **RIQL can effectively defend such effect and achieves both exceptional performance and remarkable stability**.

G Discussion of the Corruption Setting

In our corruption setting, the states and next-states are independently corrupted. However, our work does not consider the scenario where next-states are not explicitly saved in the dataset, meaning that corrupting a next-state would correspond to corrupting another state in the same trajectory.

The motivations behind our chosen corruption setting are as follows:

- Our work aims to address a comprehensive range of data corruption types. Consequently, conducting an independent analysis of each element's vulnerability can effectively highlight the disparities in their susceptibility.
- When data are saved into (s, a, r, s') for offline RL, each element in the tuple can be subject to corruption independently.
- Our corruption method aligns with the concept of ϵ-Contamination in offline RL theoretical analysis (Zhang et al., 2022), which considers arbitrary corruption on the 4-tuples (s, a, r, s').
- Data corruption can potentially occur at any stage, such as storage, writing, reading, transmission, or processing of data. When data is loaded into memory, there is also a possibility of memory corruption and even intentional modifications by hackers. In the case of TD-based offline RL methods, it is common practice to load 4-tuples (s, a, r, s') into memory and each element has the potential to be corrupted independently.

In the future, exploring the effects of data corruption in scenarios considering the dependence between states and next-states, or in the context of POMDP, holds promise for further research.

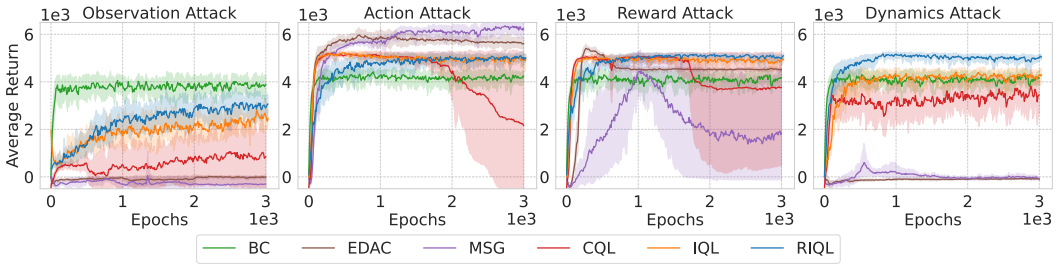

(a) HalfCheetah

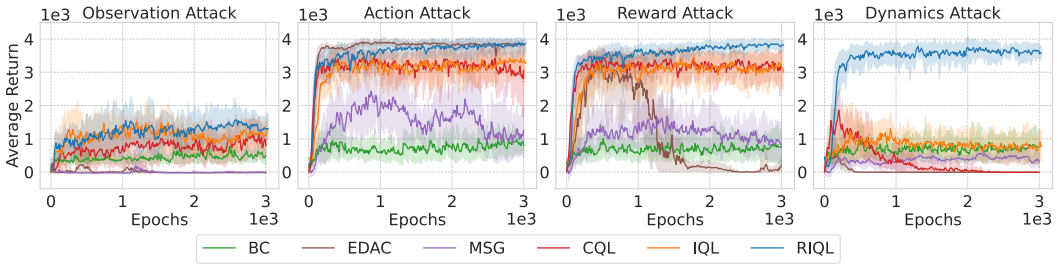

(b) Walker

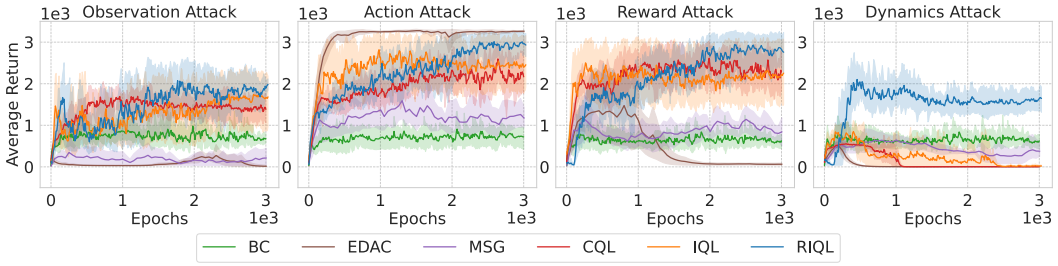

(c) Hopper

Figure 17: Learning curves under **random data corruption** on the "medium-replay" datasets.

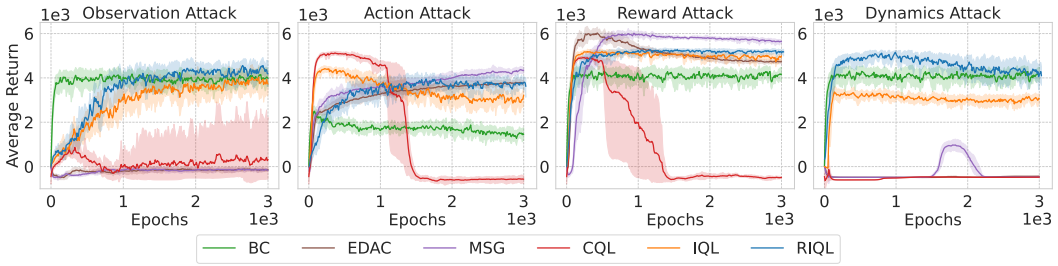

(a) HalfCheetah

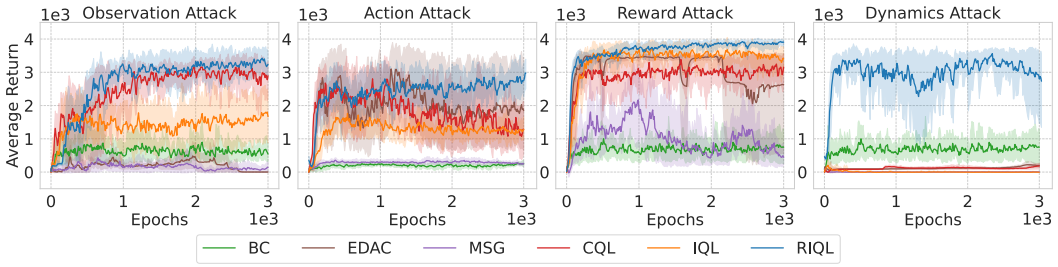

(b) Walker

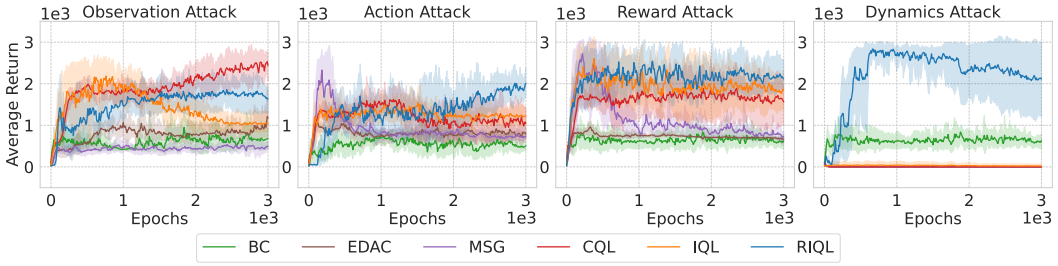

(c) Hopper

Figure 18: Learning curves under **adversarial data corruption** on the "medium-replay" datasets.